Applied Catalysis B: Environmental 162 (2015) 564–572

Contents lists available at ScienceDirect

Applied Catalysis B: Environmental

journal homepage: www.elsevier.com/locate/apcatb

MWCNT–TiO_2–SiO_2 nanocomposites possessing the photocatalytic activity in UVA and UVC

Bożena Czech[a,*], Waldemar Buda[b], Sylwia Pasieczna-Patkowska[c], Patryk Oleszczuk[a]

[a] Department of Environmental Chemistry, Faculty of Chemistry, University of Maria Curie-Sklodowska, Pl. M. Curie-Sklodowskiej 3, 20-031 Lublin, Poland
[b] Department of Adsorption, Faculty of Chemistry, University of Maria Curie-Sklodowska, Pl. M. Curie-Sklodowskiej 3, 20-031 Lublin, Poland
[c] Department of Chemical Technology, Faculty of Chemistry, University of Maria Curie-Sklodowska, Pl. M. Curie-Sklodowskiej 3, 20-031 Lublin, Poland

ARTICLE INFO

Article history:
Received 17 May 2014
Received in revised form 11 July 2014
Accepted 15 July 2014
Available online 22 July 2014

Keywords:
Photocatalysis
TiO_2
Carbon nanotubes
Phenol
Dyes

ABSTRACT

The results of studies on application of TiO_2 and SiO_2 co-precipitated in the presence of CNT to prepare the nanocomposites CNT–TiO_2/SiO_2 are presented. Nanocomposites were characterized by a large overall surface area (243–252 m^2/g), occurrence of TiO_2 in the anatase form (7–8 nm) and reduced band gap energy (from 3.2 eV to 2.2 eV). The studies confirmed the role of CNT as a factor not only increasing the overall surface area of the nanocomposites but also allowing for obtaining the systems of uniform distribution of the crystallites TiO_2/SiO_2 on their surface and those activated with visible light. Photocatalytic oxidation carried out for 2 h using the nanocomposites resulted in 75% removal of phenol (UVC irradiation) and a complete loss of methyl orange (UVA irradiation). The nanocomposites containing about 8 wt% of CNT were the most active. Removal of the phenol and methyl orange proceeded according to the first order kinetics (k_1 for UV decomposition of phenol was 0.4–0.74 × 10^{-2} min^{-1}, and for Vis removal of methyl orange 2–12 × 10^{-2} min^{-1}).

1. Introduction

The increasing interest in photocatalysis observed lately is a result of its unquestionable advantages. Under the room temperature and pressure conditions and in the presence of UV on the surface of TiO_2 there proceed some reactions leading to generation of very reactive oxide forms (ROS) i.e.: $^{*}OH$, O_2^{*-}, H_2O_2, HO_2^{*-}. ROS take part in oxidation and reduction reactions causing mineralization of organic compounds to CO_2 and H_2O or reduction of metals [1]. TiO_2 is the most common catalyst applied in photocatalytic processes because it is safe, stable, available and cheap. Disadvantages of using TiO_2 are connected with its too small activity due to the extent of band gap energy (E_g) which is about 3.2 eV in anatase [2]. Thus TiO_2 can be activated only by UV which requires expensive and energy-consuming UV lamps. In order to increase TiO_2 activity in the visible light region (to reduce the size of *Eg*), TiO_2 is modified by transition metals additives, rare earth metals, non-metals, combined with other semiconductors, sensitizers etc. [3].

Mechanism of TiO_2 surface reactions is well known and described in the literature [4]. One of the factors affecting organic compounds decomposition is their adsorption by the semiconductor surface and radiation absorption by the semiconductor. The commercially available catalyst P25 (earlier known as Degussa P25, actually Evonik) is characterized by a relatively small overall surface area in the range 50–55 m^2/g [5]. Application of a modifier which would increase the surface area should make the process more effective. Another factor affecting photocatalysis effectiveness is type and number of surface OH groups or the presence of adsorbed H_2O which gives the very reactive and non-selective radicals $^{*}OH$.

Photocatalytic activity is closely connected with the size of nanocrystallites TiO_2 [6]. One of the ways to control and slow down the crystallization process of TiO_2 [7] is co-precipitation with SiO_2, Al_2O_3, zeolites or clays [8]. The surface bond-conjugated TiO_2/SiO_2 photocatalyst offers higher photo activity, larger surface areas and higher capacities for adsorbing organics than powder TiO_2 [7].

Due to the fact that photocatalytic activity depends on the number of active sites on the surface, surface accessibility and losses caused by recombination, the activity can be increased by preparing materials which would possess an increased number of active sites, limited recombination e^-/h^+ and could be activated with visible light. This target can be reached using the TiO_2 systems modified with the addition of CNT [9].

The growing interest in the use of carbon nanotubes [10] is connected with a unique structure and chemical properties of CNT: low

* Corresponding author. Tel.: +48 81 5375545; fax: +48 81 5375565.
E-mail addresses: bczech@hektor.umcs.lublin.pl, czech.bozena@poczta.onet.pl (B.. Czech).

http://dx.doi.org/10.1016/j.apcatb.2014.07.035
0926-3373/

density, high tensile strength, high conductivity, and a high surface area to volume ratio [11]. Hence, they are used in pharmaceutics, nanocomposites, and often as stable suspensions in polymer resins.

Lately the use of carbon nanotubes as the materials applied for the increase of effectiveness of surface reactions has been more frequently observed [12].

Application of the TiO_2–CNT nanocomposites enables exploitation of the advantages of both materials—photocatalytic activity of TiO_2, adsorption capacities of CNT (surface area 200–400 m^2/g) and reduction of *Eg* after CNT doping of TiO_2. CNTs application makes TiO_2 morphology control easier. As a result, these materials are activated using visible light. However, the activity mechanism in visible light is not explicit. It is believed that the addition of CNT results in changes of the size of band gap energy of TiO_2 and/or sensitization of TiO_2. The addition of CNT increases TiO_2 activity due to inhibition of $h^+/e-$ recombination processes similarly to metals. In TiO_2, which is a semiconductor of type *n*, in the presence of CNT, photogenerated e^- can dislocate to the surface of CNT of lower Fermi level (the CNT acts as an electron sink), leaving the excess of h^+ in the valence bond of TiO_2. h^+ can migrate to the surface of TiO_2 and react making TiO_2 a semiconductor of type *p* [13]. The other mechanism is connected with the action of CNT as the photosensitizer, transferring electrons into the conduction band of the TiO_2 and permitting a reduction process. Simultaneously the positively charged CNT remove an electron from the valence band of the TiO_2, leaving a hole. The positively charged TiO_2 can then take part in an oxidation process; for example, with water to form hydroxyl radicals [12].

The key parameter of the activity of CNT–TiO_2 composites is both preparation method, the mass ratio CNTs:TiO_2, and the calcination temperature. Generally it was observed that the optimum mass ratio between CNTs and TiO_2 is in the range of 1.5–20% depending on the treated pollutant and the CNT–TiO_2 composites synthesized via the sol–gel method showed higher photocatalytic activity than the composite via hydrothermal method [14].

There are few data in the literature about synthesis and application of nanocomposites of CNT–TiO_2/SiO_2 type. The hitherto studies focused on obtaining the CNT–TiO_2 systems containing a small admixture of CNT which was a few percent [15]. In the presented studies the co-precipitation of TiO_2 and SiO_2 in the presence of CNT has been applied for the first time to prepare the nanocomposites CNT–TiO_2/SiO_2 of different CNT contents. The role of SiO_2 was the promotion of TiO_2 crystallization, stability and many other chemical parameters e.g. enhanced adsorbability through hydroxyl groups [16]. However, for the content of SiO_2 above 30%, the crystallization of anatase TiO_2 is not observed as the result of diffusion barrier of Ti atoms and though delayed nucleation [16,17]. SiO_2 has emerged as an appropriate support for improving the photocatalytic process, since it is a chemically inert material with large surface area and transparent to UV radiation [18].

The aim of the investigations was to prepare photocatalysts based on TiO_2 with photocatalytic activity toward visible region. The addition of CNT in the amount of 0.15–17.8 wt% was to enhance adsorbing capacity of the photocatalyst and its activity toward visible light decreasing the *Eg* value. The photocatalytic activity of the studied materials was determined based on methyl orange and phenol removal from waste waters which are model contaminants removed in the process measuring photocatalysis effectiveness.

2. Materials and methods

2.1. Materials

Titanium buthoxide (TBOT) and tetraethyl orthosilicate (TEOS) were purchased from Sigma-–Aldrich (Poland) and used for CNT–TiO_2/SiO_2 nanocomposites preparation. Functionalized carbon nanotubes (MWCNT–COOH, outer diameter 20–30 nm, length 10–20 μm, surface area >110 m^2/g, —COOH Content 1.23 wt%) were received from Timesnano (China). Ethanol (absolute) and butanol were purchased from POCH (Poland). The model solution of dye containing 10^{-3} mol/L of methyl orange (POCH, Poland) or 0.0264 mol/L of phenol (POCH, Poland) was prepared using distilled water.

2.2. Photocatalysts preparation

The photocatalysts were prepared by ultrasonic assisted sol–gel method. TBOT (10 mL, 29.38 mmol) was mixed with TEOS (1.64 mL, 7.35 mmol). The mixture was sonicated 10 min than adequate amount of CNTs was added into solution. The suspension was sonicated four times for 15 min and hydrolyzed by adding 100 mL of ethanol: butanol (9:1) mixture containing 3.3 mL of water. After hydrolysis the suspension was additionally sonicated twice time for 15 min and was treated hydrothermally at 60 °C for 24 h. After decantation the solid was washed with distillated water (10 mL), dried for 12 h at 110 °C. The prepared nanocomposites had following molar composition: TiO_2:SiO_2:MWCNTs – 1:0.25:*x* (*x* = 0.01–0.6) and are denoted as WB1-60, where number corresponds to the molar ratio of CNT. The loss of CNT during preparation could not be observed as the co-precipitation of TiO_2 and SiO_2 was conducted in CNT suspended medium.

2.3. Photocatalytic test

The activity of the photocatalysts was tested in the photocatalytic oxidation of organics. As the pollutant methyl orange (MO) and phenol (Ph) were used. During the kinetic studies of filtered samples were analyzed by UV–Vis spectroscopy. The UVA activity of nanocomposites was measured in the process of the photocatalytic oxidation of Ph and UVC activity—for MO in the photochemical reactors equipped in one of the lamps. For UVA studies of 10 mg/L Ph the low pressure mercury lamp (light centered at 254 nm, 15 W) was applied in tube reactor. The UVC–Vis studies were conducted using medium pressure lamp (150 W) emitting at: λexc = 254, 313, 366 (main), 405, 436, 546 and 578 nm in Heraeus, 0.75 L reactor. The UV light below 300 nm was filtered.

The model solution of 1×10^{-3} mol/L MO or 10 mg/L Ph and 0.5 g/L of the photocatalyst was placed in the reactor, magnetically stirred (500 rpm) and kept in dark for 30 min to obtain the equilibrium. The first sample was collected in the end of "dark" period, and then samples were collected, in the regular intervals, for 2 h. Filtered samples were analyzed by UV–Vis spectroscopy.

The dye concentration was spectrophotometrically measured in Varian Cary 4000 Spectrophotometer: scan rate 600 nm min^{-1}; time response: 0.1 s; spectral band 2 nm. The linear correlation between absorbance and concentration was tested using solutions at 0–1×10^{-3} mol/L MO or 1–10 mg/L Ph) concentrations with the linear response over the whole range of considered concentrations. The concentration of studied pollutants was measured from the absorbance at the proper wavelength: λ = 535 nm for MO and λ = 270 nm for Ph by using calibration curves. The results describing the removal of Ph or MO were presented as c/c_0, where *c* was the concentration of MO or Ph determined at time *t* and c_0 was initial concentration of MO or Ph. UV activity of the studied nanocomposites was described in detail for Ph removal, and Vis activity for MO photodecomposition.

2.4. Catalysts examination

The nanocomposites were characterized by the following physicochemical methods: (1) the specific surface area of the

nanocomposites was determined on the basis of low-temperature nitrogen adsorption–desorption method in AUTOSORB-1CMS (Quantachrome Instruments, USA). S_{BET} were calculated using the standard BET method for nitrogen adsorption data and pore size distribution was obtained from desorption branch of the isotherm according BJH procedure, (2) the composition of the nanocomposites and crystal size of TiO_2 was measured by XRD on Empyrean (PANalytica, Netherland) using monochromatic Cu Kα radiation, (3) the thermogravimetric analysis (TGA and DTG) was carried out with TG/DTA/DSC Setsys 16/18, (4) SEM studies were conducted on a Phenom FEI microscope operating at 15.0 keV, (5) for surface layer characterization infrared photo acoustic (mid-IR PA) spectroscopy was applied using Bio-Rad Excalibur 3000 MX spectrometer equipped with photo acoustic detector MTEC300 (in the helium atmosphere in a detector), (6) Raman spectroscopy was applied using inVia Reflex, Renishaw, UK, (7) The UV–Vis spectra were recorded on a Jasco V-660 spectrophotometer fitted with a PIV-756 diffuse reflectance accessory using ZnO as a reference. Detailed information about method used for nanocomposites characterization is presented in supporting information.

3. Results and discussion

3.1. The physicochemical properties of nanocomposites

Fig. 1S presents the adsorption–desorption isotherms and pore distribution of the catalysts under investigations. The isotherms of all catalysts are of IV type with a two-segment hysteresis loop of IV type according to the IUPAC classification [19].

With the increasing content of CNTs in nanocomposites, pore distribution becomes more bimodal. As follows from the data in Table 1, the nanocomposites prepared by the sole–gel method are characterized by a large surface area decreasing insignificantly with the increase in the CNT content and relatively large diameters of mesopores.

A relatively large overall surface area of nanocomposites is caused by the presence of nanotubes which enable better dispersion of TiO_2 thereby not promoting aggregation [20].

3.1.1. XRD

The XRD spectra of initial MWCNT and prepared nanocomposites are presented in Fig. 1. In the CNT spectrum there are present two well-formed reflections for the angles $2\theta \approx 25.96^\circ$ and $2\theta \approx 42.93^\circ$, assigned to the (0 0 2) and (1 0 0) reflections of the CNT lattice, confirming the concentric-cylindrical behavior of nanotubes structure and hybridization of sp^2 atoms [21]. The addition of MWCNT to the TiO_2–SiO_2 system does not induce changes in nanotubes morphology but only modifies the surface.

According to the database JPD 21-1272, the peaks present in the spectrum for $2\theta = 25.2$, 37.9, 48.3, 53.8, 62.7, 68.9, 70.1 and 74.8 come from the anatase crystallites. Similar to [22], there was observed slight broadening of the peak for $2\theta = 25.2^\circ$ on the XRD spectra due to superposition of the signals originating from anatase (25.2°) and MWCNT (25.96°). SiO_2 cannot be observed in XRD that was the result of applied Ti:Si ratio [16]. The size of anatase crystallites was calculated using the Scherrer equation ($d = 0.9\lambda/\beta^* \cos\theta$ where $\lambda = 0.154$ nm, β – peak broadening, θ – the diffraction angle). The studied catalysts differ insignificantly in the size of anatase crystallites but it can be seen that their size decreases with the increasing CNT content, probably as a result of hydroxyl groups' interactions in the titanium precursor and COOH groups in CNT. This is probably caused by transition from the systems with nanotubes dispersed in the lattice TiO_2–SiO_2 (WB1–WB20) to the systems with the TiO_2–SiO_2 crystallites deposited on the outer surface of carbon nanotubes (WB40, WB60).

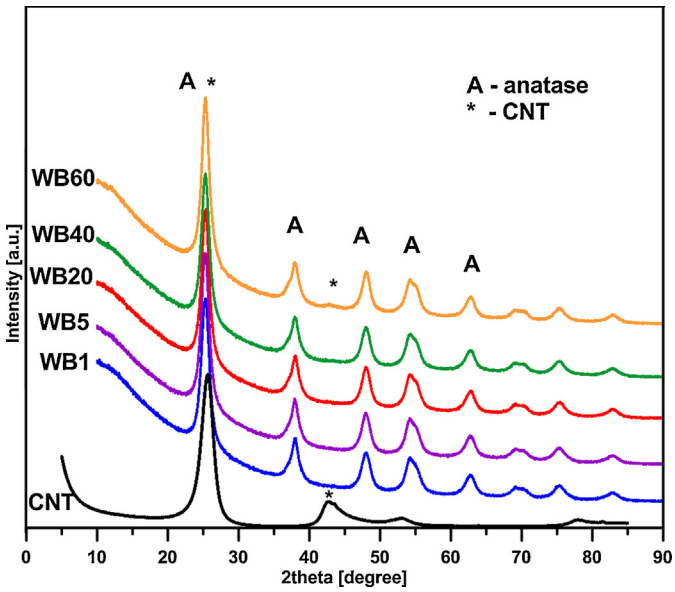

Fig. 1. The XRD spectra of studied photocatalysts: A – anatase peaks, * – CNT characteristic peaks.

3.1.2. SEM

CNTs affect TiO_2 morphology and TiO_2 agglomeration. SEM technique was used for the determination of the CNT localization in the nanocomposites. The SEM spectrum (Fig. 2) shows spherical particles of TiO_2 composed of nanotubes of a diameter about 10 nm which is also confirmed by calculations from XRD. Nanocomposites possess a cloddish structure and the primary crystallites TiO_2/SiO_2 have a tendency toward agglomeration. Clusters are formed with the increasing CNT's contents. In the composites with a small contribution of CNT (WB1–WB20), the nanotubes are inside the crystallites TiO_2/SiO_2 or "lie" on the surface of TiO_2/SiO_2 forming "antennas" directed outward.

The nanotubes protrude above the grains surface in different directions in the catalysts with a large content of CNT (WB40–WB60). With the increasing content of nanotubes, the size of TiO_2 crystallites decreases. A similar dependence was observed by [22]. The nanocomposites of large CNT content, obtained by the sol–gel method, are characterized by homogeneous distribution of the TiO_2/SiO_2 crystallites on the surface of nanotubes. This confirms the role of CNT as a factor not only increasing overall surface area of the nanocomposites but also allowing to obtain the systems of uniform distribution of TiO_2/SiO_2 crystallites on their surface [7].

Taking into account the share of nanotubes in the studied structure, they can be divided into two main groups: (1) catalysts of up to 3.5 wt% content of nanotubes in which they play a role of the admixture diffused inside the TiO_2/SiO_2 nanocrystallites and (2) catalysts of over 4 wt% content of CNT which are the supports of TiO_2/SiO_2 crystallites localized on the outer surface of nanotubes.

3.1.3. DTG/TGA

The TGA thermograms show that the presence of CNT induces formation of smaller thermal resistance material (Fig. S2A). During heating at the temperature exceeding 400 °C, there is observed nanotubes decay which lasts up to the time of their total oxidation at 636 °C. Thermal decomposition of nanocomposites (containing over 1 wt% of CNT) was found at 634 °C and the decomposition temperature decreased up to 446 °C in the case of large content of nanotubes (17.5 wt%). As follows from the data, the presence of CNT affects significantly the thermal decomposition of the nanocomposites. The systems containing a small amount of CNT (up to 1 wt%) are characterized by large temperature resistance and do

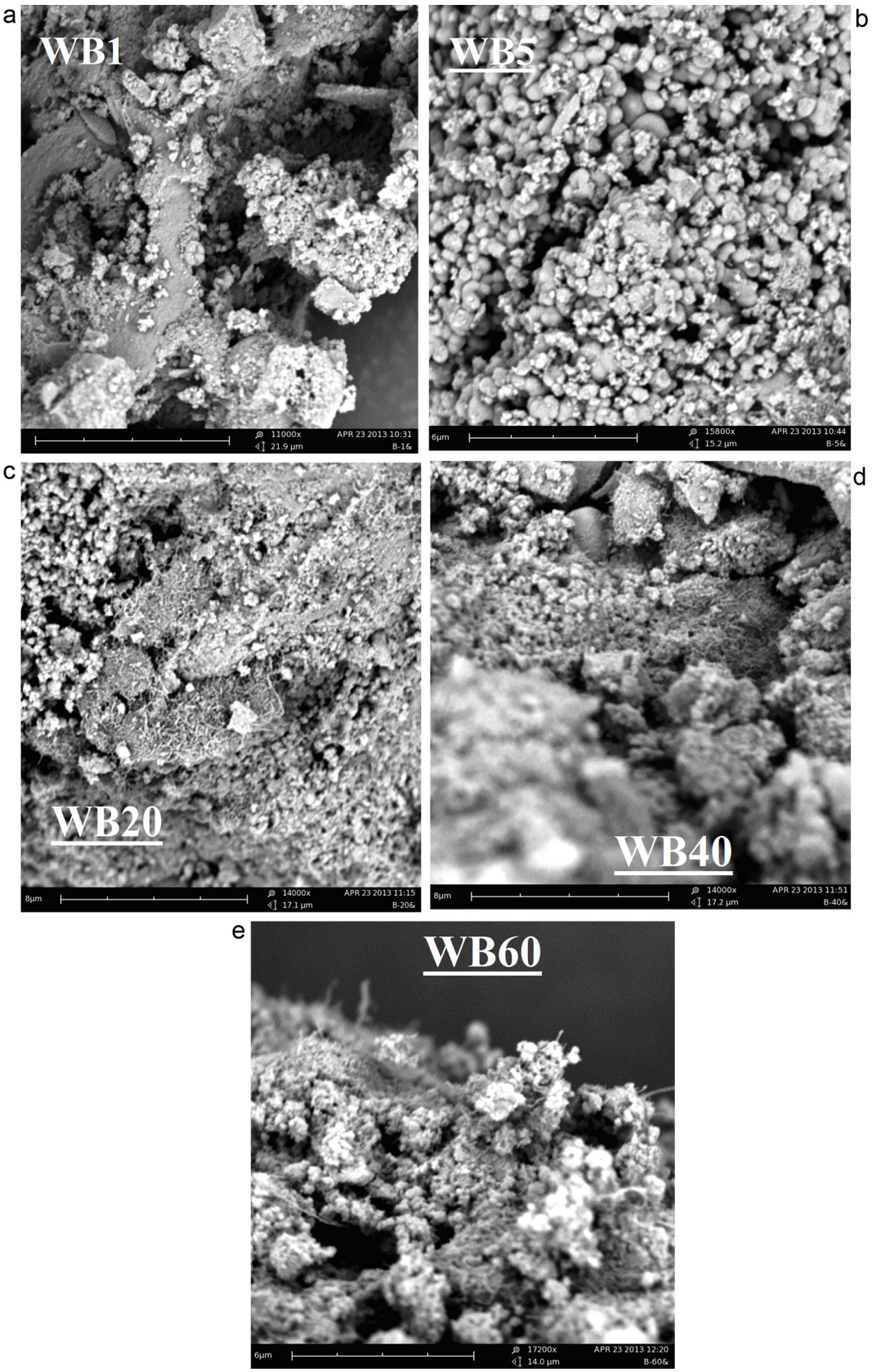

Fig. 2. SEM micrographs of studied nanocomposites.

Table 1
The properties of nanocomposites studied.

Catalyst	S_{BET} [m^2/g]	Pore diameter [nm]	CNT molar ratio	CNT concentration [wt%]	Anatase crystal size [nm]
WB1	252.36	63.71	0.01	0.15	7.8
WB5	251.54	69.98	0.05	0.75	7.3
WB20	245.32	69.93	0.20	3.48	7.2
WB40	249.53	68.75	0.40	8.78	7.2
WB60	243.60	76.31	0.60	17.8	6.7

not change in a wide temperature range. Beginning with WB20 with the CNT content increase (over 3 wt%), the systems strength decreases, particularly at 650 °C [23].

On the DTG thermograms (Fig. S2B) two peaks corresponding to the two-stage mass loss can be seen. The first loss, almost the same for each nanocomposites (73–88 °C) is connected with the desorption of physically adsorbed water. The other mass loss (~650 °C) resulting from CNT's combustion is shifted toward lower temperatures with the increasing content of CNT in the nanocomposites. In raw nanotubes the process of their decomposition starts at 420 °C and reaches maximum at 609 °C. All in all, the addition of CNT decreases thermal resistance of the material at temperatures above 450 °C which does not exclude practical application of materials of this type.

3.1.4. FT-IR/PAS

Figs. S3A and S3B present the FT-IR/PAS spectra of the studied systems. On all of them there can be seen a wide band in the range 3600–3100 cm^{-1} with the maximum at about 3400 cm^{-1} of different intensity which indicates the presence of OH groups originating from physically adsorbed water, also confirmed by a band at about 1600 cm^{-1}. This band may also indicate the presence of Ti—OH groups [24]. Intensity of the band in the range 3600–3100 cm^{-1} decreases with the increasing CNT content which is the evidence for the increase of surface hydrophobicity of the materials.

On the spectra of the samples WB1, WB5 and WB20 also the band with the maximum at about 3735 cm^{-1} assigned to vibrations of the isolated hydroxyl groups Si—OH [25] resulting from TiO_2 and SiO_2 co-precipitation. The presence of SiO_2 is confirmed by the bands at 1050 cm^{-1} and 810 cm^{-1} (asymmetric and symmetric vibrations of the Si—O—Si group). On the spectra of WB1, WB5 and WB20 samples also the band of low intensity at about 3690 cm^{-1} assigned to the Ti—O—Ti groups can be seen [26]. With the increasing share of nanotubes in the studied catalysts, the bands coming from TiO_2 and SiO_2 disappear in their spectra FT-IR/PAS but new bands characteristic of raw carbon nanotubes appear. The peaks at 3515, 3440 and 3350 cm^{-1} indicate the presence of OH groups coming from the COOH group. The bands in the range 1250–1000 cm^{-1} also confirm the presence of COOH groups on the catalysts surface (vibrations of the C—O group). Intensity of the band at 1400 cm^{-1} remains practically unchanged, independent of CNT content in the sample. This band is assigned to the presence of OH groups, carboxyl–carbonate structures, vibrations of aliphatic groups CH_3 [27] and Ti—O groups [24]. The presence of the last ones is evident in the spectra of CNT-doped samples but not found in the FT-IR/PAS ones of raw CNT [28].

3.1.5. Raman spectroscopy

Due to the absence of carbon peaks in the powder XRD diffraction patterns, Raman spectra were recorded to confirm the structure of synthesized nanocomposites as illustrated in Fig. S4. The Raman spectrum of all investigated materials possesses two sets of four modes assigned to TiO_2 and MWCNT's respectively. The first set of four peaks consists of the well resolved intense peak at 160 cm^{-1} and three overlapping peaks at 399 cm^{-1} (B_{1g}), 521 cm^{-1} (B_{1g}), 620 cm^{-1} (E_g) assigned to anatase [29]. The second one exhibits two pairs of first and second order spectra of carbonaceous materials. Well resolved first order peaks with the intensity maxima at 1346 cm^{-1} and 1582 cm^{-1} are related to imperfection in the carbon nanotubes structure (band *D*) and are also attributed to the vibrations of sp^2 bonded carbon atoms (band *G*) [30]. The *D*-band intensity is proportional to defect density. The *G*-band is a result of C—C bond stretching typical to sp^2 hybridizations found in graphitic carbon [31].

The second order spectra also exhibit two peaks. The first at nearly 2697 cm^{-1} (*D'*) assigned to the first overtone of band *D* and the second *G'* at 2959 which is a combination of *D* and *G* modes [30]. It is noteworthy that the increase of CNT's content in composites causes changes in relative intensity of anatase spectrum. However they are observed even in the spectrum of catalyst with large nanotube contents. The ratio of the *D*-band and *G*-band intensities (*ID*/*IG*) is often used to quantify the defectiveness of CNTs, and this ratio can be used to estimate the thermal stability of CNTs [32]. MWCNTs with $ID/IG > 0.60$ corresponded to weak CNTs, and CNTs with $ID/IG \leq 0.60$ to strong CNTs. The observed parameters varied: 1.12; 1.16; 1.08; 1.21; 1.02 for WB1, WB5, WB20, WB40 and WB60, respectively. Thus there was created the material of a large number of defects in CNT which suggests increased activity of the prepared photocatalysts.

3.1.6. UV–Vis/DRS

The effect of the CNT addition to the TiO_2/SiO_2 system on the activity of the catalysts in visible light was determined using the UV–Vis/DRS spectroscopy. The size of band gap energy was estimated by means of the Tauc method andcalculated according to the Kubelka–Munk equation (Eq. (1)):

$$K = \frac{(1 - R^2)}{2R}, \quad (1)$$

where *K* is the reflectance calculated according to the Kubelka–Munk equation, *R* is the reflectance obtained from the UV–Vis (%) spectrum presented in Fig. 3. The quantity *Eg* is given in Table S1.

Even a small addition of MWCNT decreases the catalysts' *Eg* quantity. Fig. S5 presents the dependence of change of *Eg* in a function of MWCNTs amount in the catalyst. In the concentration range 0.15–12.62 wt%, a linear drop to the minimal *Eg* value 2.185 eV is observed ($R^2 = 0.998$). The decrease in the band gap energy suggests larger photocatalytic activity of the studied catalysts in visible light [33].

3.2. Photocatalytic test and photodegradation kinetics of phenol

The effectiveness of UV purification of water containing phenol presented as a loss of phenol concentration in time (Fig. 4) indicates that the addition of CNT can increase the system activity only after applying nanocomposites containing at least 0.5 wt% in the photocatalyst. The irradiation with longer wavelengths resulted in increased Ph removal (Fig. S6). Only about 10% decrease in the phenol concentration was obtained in the studies carried out in the dark which confirms the fact that the role of CNT in nanocomposites is not exactly increase of adsorbing capacity but rather increase of

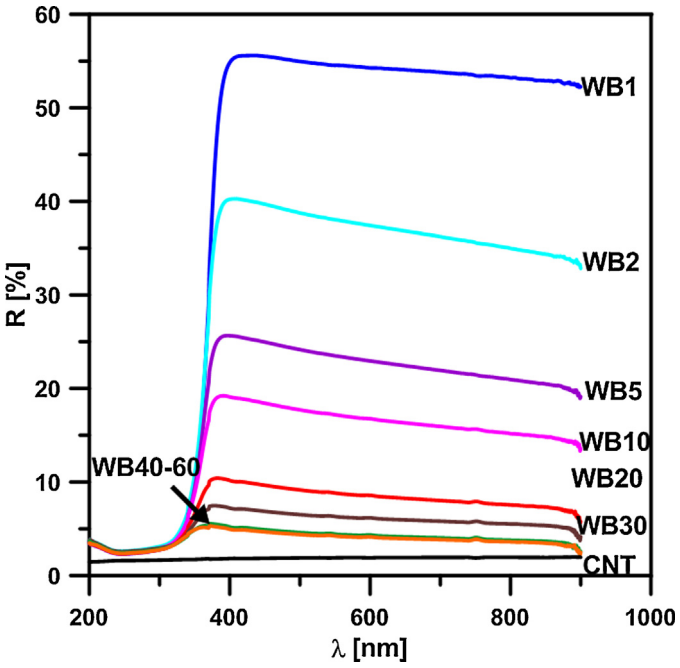

Fig. 3. UV–Vis/DRS spectra of studied nanocomposites.

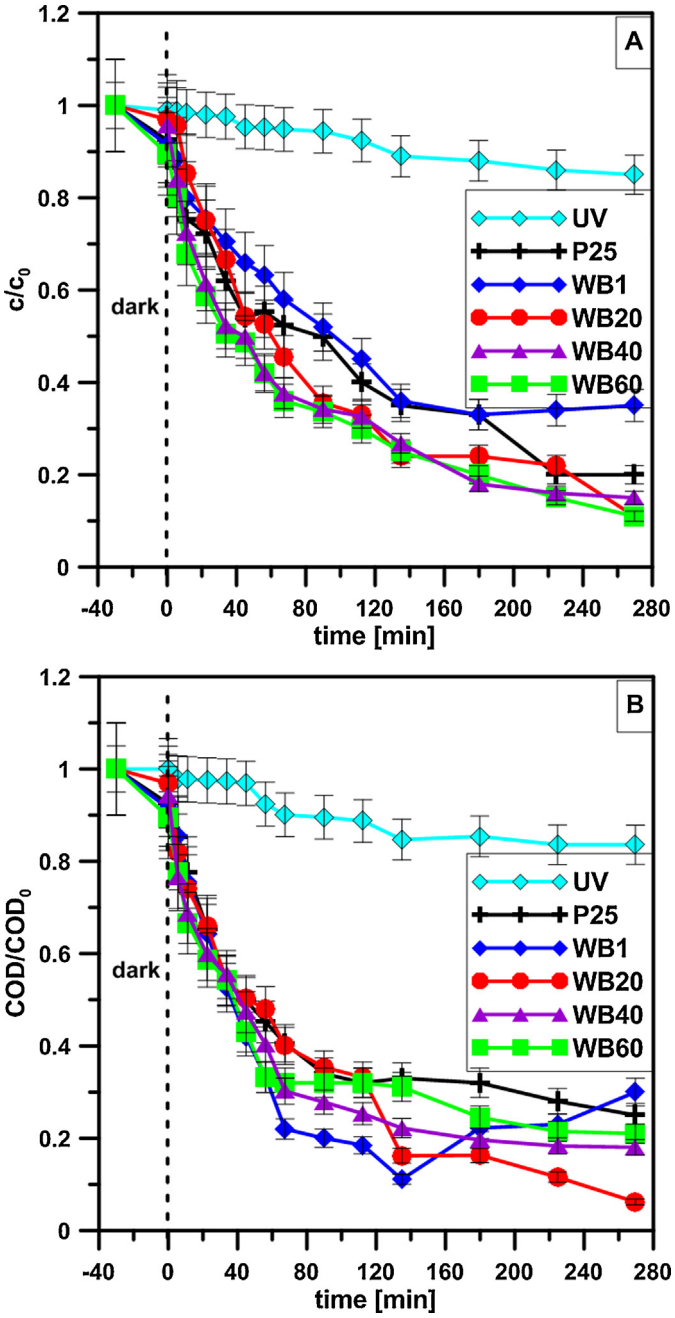

Fig. 4. Phenol photoremoval described as decrease of the phenol concentration (a) and COD of phenolic wastewater treated photocatalytically.

photocatalytic activity of TiO_2 after exposure due to better electric charge transfer that is a smaller *Eg* quantity [12].

The increase of UV activity results from the supporting character of CNT. Fig. 4A shows clearly that the process of phenol removal using commercially available P25 and the catalysts obtained in this study (WB1, WB20, WB40 and WB60) proceeds in a similar way for the first 60 min. Later there appear some differences among the catalysts and P25 pointing out to better effectiveness of WB20, WB40 and WB60 than P25. WB1 proved to be the least productive photocatalyst, similar or even worse than P25. As follows from the obtained data, the contribution of phenol photolysis to decomposition of phenol in water was small. Generally, the application of more CNT in TiO_2, especially above 8 wt%, promoted the Ph photooxidation. There are two reasons for the increased activity of nanocomposites: (1) e^- formed due to excitation migrate to the nanotubes, (2) CNTs affect inhibition of e^-/h^+ recombination in TiO_2. Another factor affecting increased phenol removal was applying the systems of larger adsorbing capacity compared to that of P25 thus of a larger number of active sites. The expanded surface due to CNT application allows larger adsorption of hydroxyl groups being a source of *OH radicals [23]. O_2, taking part in the process and adsorbed on the CNT surface, is also a source of radicals in the reaction with e^-. Taking all these aspects into consideration, there are more hydroxyl radicals in the TiO_2–CNT system than in TiO_2 [24], which confirms intensifying effect of CNT.

In the case of phenol and its oxidation products removal, expressed as a total parameter, COD, the greatest changes in water quality are found during the first 45–60 min of the treatment process (Fig. 4B). It should be highlighted that in this period the range of COD changes in the presence of studied photocatalysts is similar. There is observed intensive decay of phenol molecules and then the products of relatively low susceptibility to decomposition (hydroquinone and benzoquinone) [34] are formed. Due to UV radiation, only about 18% decrease in the COD parameter value is observed indicating low susceptibility of these compounds to UV photolysis. Application of the photocatalysts significantly improves water quality. The best effect is found for the systems of small or intermediate content of nanotubes (WB1, WB20). Thus nanocomposites of CNT content to about 10 wt% are characterized by better mineralization capacity than TiO_2 itself.

The obtained results show that at medium contents of nanotubes, the process of phenol removal is enhanced and the intermediate oxidation products undergo faster decomposition using the systems of nanotube contents of the order 1–8 wt%. Prolongation of UV radiation with the simultaneous use of larger number CNT (WB40, WB60) proceeds in a similar way. At the time when the amount of CNT is relatively large, they "blanket" the composites surface against UV radiation decreasing the number of *OH radicals. In turn, this causes the increase of the rate of e^-/h^+ recombination or deficit of radicals which could take part in decomposition of more resistant transition products of phenol oxidation. The covering and shadowing effect of CNT excess is observed in literature [35]. The nanocomposites containing 8–17 wt% are

characterized by the largest activity which is in a good agreement with the data (about 10 wt%) obtained by Chen et al. [36] during however photoelectrocatalytic degradation of phenol.

Decrement of phenol concentration, c, during the treatment time, t, using the CNT–TiO_2 systems was described by the pseudo first order kinetics based on equation [2]:

$$r = -\frac{dc}{dt} = kc^n \tag{2}$$

where r, c and t represent the rate of degradation, methyl orange or phenol concentration and time respectively. Also k and n are the rate constant and reaction order.

To simplify the heterogeneous photocatalytic process the initial concentration of the organic substrate c_0 was kept constant. The apparent pseudo first-order rate constant (min^{-1}) k_1 was obtained by fitting the experimental data from the relation (Eq. (3)):

$$-\ln\left(\frac{c}{c_0}\right) = k_1 \cdot t \tag{3}$$

The values of k_1 were determined from the slope of the linear regressions obtained by plotting—$\ln(c/c_0)$ versus time. The other constants: apparent rate constants of the catalyst per mass unit (k_w) and per surface area unit (k_s) were estimated from Eqs. (4) and (5):

$$k_w = \frac{k_1}{c_w \cdot V_r} \tag{4}$$

$$k_s = \frac{k_1}{S_{BET} \cdot c_w \cdot V_r} \tag{5}$$

where c_w was the concentration of the photocatalysts, S_{BET} BET surface of photocatalyst and V_r – the reactor volume (1 L for the tube reactor and 0.75 L for the batch reactor). Consequently, half-lives were calculated using Eq. (6):

$$t_{1/2} = \frac{0.6934}{k_1} \tag{6}$$

Table 2 presents the obtained results of calculations.

Taking into consideration the kinetic data, the largest values k_1 were obtained during phenol removal using WB20 and WB40. Those values are nearly twice as large as for WB1. This indicates that in the case of WB1 for which the relatively smallest value R^2 was obtained, this process can be described by the first order kinetics only in some range. The values of kinetic constants for the studied nanocomposites are larger by one order than those obtained by Li et al. [37] which were 1.19×10^{-4}, pointing out to large applicability of the studied nanocomposites in photocatalytic phenol removal from water. Considering changes of $T_{1/2}$ depending on the CNT weight content—in the case of phenol, the addition of CNT prolongs purification time contrary to the case of COD (Fig. S7). Thus the decay of organic compound takes place quickly and the oxidation products are more resistant to decomposition.

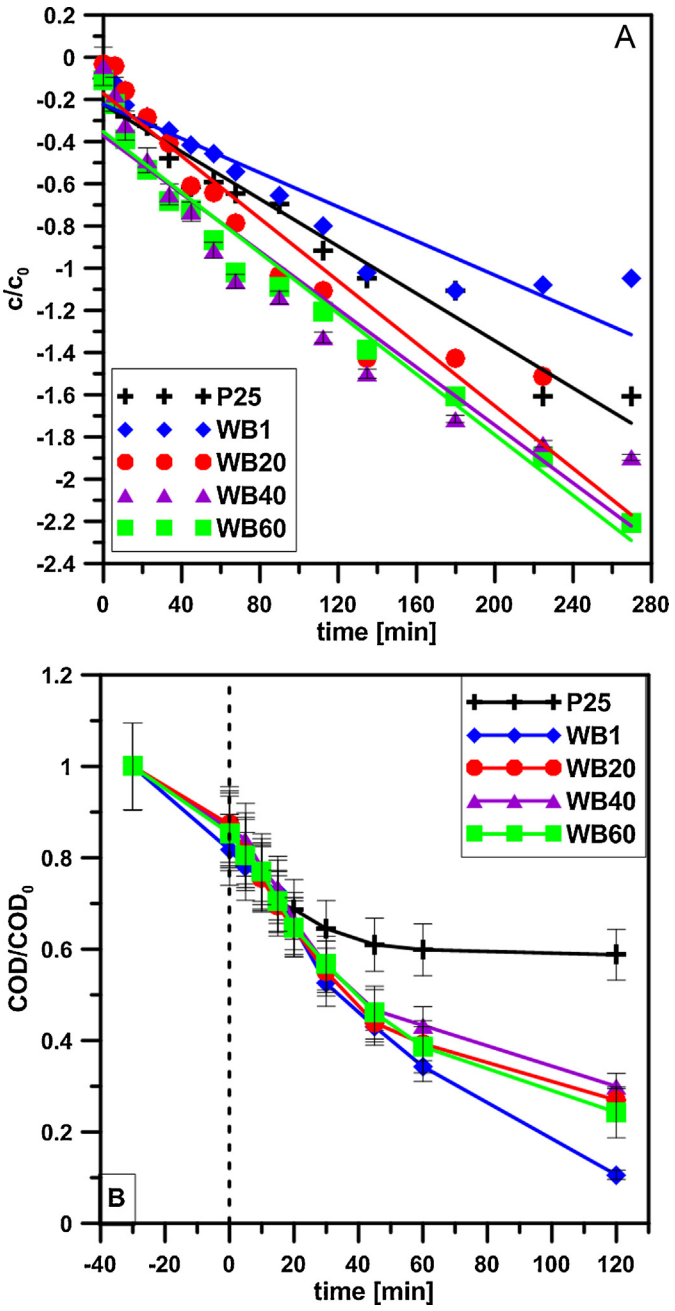

Fig. 5. (A) The changes of the methyl orange (1×10^{-3} mol/L) under Vis illumination using studied photocatalysts (0.5 g/L), (B) COD of methyl orange wastewater treated photocatalytically.

3.3. Photocatalytic degradation kinetics of methyl orange

MO was removed from the water by the studied nanocomposites very efficiently both using UV (Fig. S8) and Vis (Fig. 5). Our earlier studies during irradiation with the Vis light without a photocatalyst showed that methyl orange has a relatively poor susceptibility to decomposition under the influence of light (concentration decrease by about 10–15%). Distinctly higher effectiveness was observed in the photocatalytic systems. Regardless of the applied materials (WB1, WB40, P25), the catalytic process of bleaching proceeded with a similar efficiency during the first 20 min of treatment.

Further Vis irradiation resulted in larger removal of methyl orange using nanocomposites compared to P25. Finally, after the 2-h radiation, there was found complete removal of methyl orange after applying WB1 and 80% loss of its concentration after applying WB40. Methyl orange removal after applying P25 was 55%. As follows from the research results too large share in the composite can restrain removal of contaminants. Lower effectiveness in the case of higher CNT contents may be due to the decrease of activity in visible light of such nanocomposites as a result of photon scattering caused by surplus carbon in the photocatalyst [38]. The most effective nanocomposites of methyl orange decomposition are the systems containing TiO_2 and CNT in the amount below 8 wt%. Increased activity of nanocomposites compared to pure TiO_2 results from the earlier mentioned CNTs conductivity which taking part in inhibition of e^-/h^+ recombination are effective e^- acceptors and in the reaction with oxygen adsorbed on them enable formation of additional $^*OH$ radicals [38].

Table 2
Pseudo-first order reaction rate constants (k_1) per gram of catalyst (k_w) and per unit surface area of catalyst (k_s) of the photocatalytic oxidation of studied pollutants.

Photocatalysts	k_1 [$\times 10^{-2}$ min^{-1}]	$T_{1/2}$ [min]	k_W [$\times 10^{-2}$ min$^{-1} \times$ g^{-1}]	k_S [$\times 10^{-3}$ min$^{-1} \times$ m^{-2}]	R^{2-}
Phenol					
P25	0.56 ± 0.125	124	1.120	0.215	0.9610
WB1	0.405 ± 0.125	171	0.810	0.032	0.8751
WB20	0.741 ± 0.125	94	0.740608	3.019	0.9424
WB40	0.686 ± 0.125	101	1.373	0.055	0.9012
WB60	0.718 ± 0.125	96	1.437	0.059	0.9652
Methyl orange					
P25	0.44 ± 0.3729	158	1.173	0.235	0.8527
WB1	2.05 ± 0.128	34	5.467	0.217	0.9627
WB20	1.51 ± 0.128	46	4.024	0.164	0.9831
WB40	12.32 ± 0.128	6	32.85	1.317	0.9540
WB60	1.82 ± 0.128	38	4.85	0.199	0.9991

COD of wastewater containing MO was reduced after photocatalytic treatment. The composite with the lowest CNT content turned to be the most active in the removal of COD of MO wastewater (Fig. 5B). The same shape of all curves indicated for the same mechanism of MO photooxidation. The COD reduction corresponds directly with MO removal indicating that high surface area of nanocomposites is key parameter enhancing the photocatalytic activity of TiO_2. Lower TiO_2 activity was obviously connected with the applied UVC–Vis radiation. Although the *Eg* of nanocomposites was lower with increasing CNT content, the direct correlation was not observed. The enhanced TiO_2 activity was the result of adsorptive properties of supports that enabled the intermediates adsorption and oxidiation. The disadvantage of TiO_2-coated activated carbon is that a part of UV rays irradiating the catalysts seem to be weakened by absorption of activated carbon surface and so fewer amounts of activated species may be generated at the TiO_2 surface [37].

Taking into consideration the process kinetics, the changes of bleaching while applying the CNT–TiO_2 nanocomposites can be described by the pseudo first order kinetics. The highest value was obtained for WB40 (12.32×10^{-2} min^{-1}) (Table 2). Other nanocomposites revealed similar activity and the obtained k_1 were comparable ($1.5–2 \times 10^{-2}$ min^{-1}).

The obtained data confirmed the decomposition of methyl orange with participation of both TiO_2 and CNT. Additionally, CNTs increase the amount of adsorption of the contaminants on the surface, as in the case of using other carbon materials that is active carbon and TiO_2 [37]. The earlier studies [22] of NO oxidation also confirmed that the systems containing up to about 8 wt% CNT are characterized by the best activity.

Activity in visible light is a result of the presence of defects or contaminants in the photocatalyst lattice as well as of recombination inhibition. Thus smaller activity can be caused by faster e^-/h^+ recombination formed under the visible light radiation, thus accounting for different behavior of nanocomposites after the exposure to UV and visible light [9]. Greater effectiveness of nanocomposites compared to TiO_2 results also from character of the medium in which measurements were made (pH about 6.5) as based on the earlier studies [34], CNTs/TiO_2 systems are more effective in the inactive and alkaline ranges of pH and less effective in the acidic medium.

Greater activity of the systems containing a small admixture of CNT in visible light results from the proper proportion between the content of CNT, amount of TiO_2 and its accessibility or from masking the TiO_2 surface. When TiO_2 is a main active phase, too large amount of CNT will mask the access to active sites on TiO_2.

4. Conclusions

Summing up, it was found that (1) the obtained nanocomposites contain TiO_2 as the anatase nanocrystals; (2) the addition of CNT to the catalyst increases the hydrophobity of TiO_2 surface; (3) silica enables obtaining relatively uniformly dispersed TiO_2; (4) the addition of CNT causes increase in the activity of TiO_2 systems in the ranges of both UV and UVA (synergetic effect of CNT and TiO_2) whereby the optimal value seems to be about 8–10 wt% of CNT; (5) with larger share of nanotubes in the nanocomposite access to the light is masked which reduces its effectiveness in the methyl orange decomposition; (6) in the case of tested compounds, the task of CNT in the nanocomposite was not exactly increase of adsorbing capacities but inhibition of e^-/h^+ recombination and increase in the number of formed *OH radicals. Thus CNT in the tested nanocomposites does the task of a photosensitizer; (7) based on the studies it can be stated that the CNT–TiO_2 nanocomposites can potentially become an effective material for removal of also other contaminants from waters and waste water.

Appendix A. Supplementary data

Supplementary data associated with this article can be found, in the online version, at http://dx.doi.org/10.1016/j.apcatb.2014.07.035.

References

[1] K. Nakata, A. Fujishima, J Photochem. Photobiol. C: Photochem. Rev. 13 (2012) 169.
[2] J.-M. Herrmann, Appl. Catal. B: Environ. 99 (2010) 461.
[3] L. Sikong, M. Masae, K. Kooptarnond, W. Taweepreda, F. Saito, Appl. Surf. Sci. 258 (2012) 4436.
[4] D. Friedmann, C. Mendive, D. Bahnemann, Appl. Catal. B: Environ. 99 (2010) 398.
[5] J.A. Rengifo-Herrera, J. Kiwi, C. Pulgarin, J. Photochem. Photobiol. Chem. 205 (2009) 109.
[6] X. Li, H. Zhang, X. Zheng, Z. Yin, L. Wei, J. Environ. Sci. 23 (2011) 1919.
[7] C. Hu, Y. Tang, J.C. Yu, P.K. Wong, Appl. Catal. B: Environ. 40 (2003) 131.
[8] Y. Yu, J.C. Yu, J.-G. Yu, Y.-C. Kwok, Y.-K. Che, J.-C. Zhao, L. Ding, W.-K. Ge, P.-K. Wong, Appl. Catal. Gen. 289 (2005) 186.
[9] M.Y. Guo, F. Liu, Y.H. Leung, A.M.C. Ng, A.B. Djurišić, W.K. Chan, Curr. Appl. Phys. 13 (2013) 1280.
[10] P. Yi, K.L. Chen, Environ. Sci. Technol. 47 (2013) 12211.
[11] E.J. Petersen, L. Zhang, N.T. Mattison, D.M. O'Carroll, A.J. Whelton, N. Uddin, T. Nguyen, Q. Huang, T.B. Henry, R.D. Holbrook, K.L. Chen, Environ. Sci. Technol. 45 (2011) 9837.
[12] R. Leary, A. Westwood, Carbon 49 (2011) 741.
[13] J. Safari, S. Gandomi-Ravandi, J. Mol. Struct. 1065–1066 (2014) 241.
[14] S.M. Miranda, G.E. Romanos, V. Likodimos, R.R.N. Marques, E.P. Favvas, F.K. Katsaros, K.L. Stefanopoulos, V.J.P. Vilar, J.L. Faria, P. Falaras, A.M.T. Silva, Appl. Catal. B: Environ. 147 (2014) 65.
[15] H. Omidvar, F.K. Mirzaei, M.H. Rahimi, Z. Sadeghian, New Carbon Mater. 27 (2012) 401.
[16] B. Louis, N. Krins, M. Faustini, D. Grosso, J. Phys. Chem. C 115 (2011) 3115.
[17] C. Shifu, C. Gengyu, Surf. Coat. Technol. 200 (2006) 3637.
[18] B. Llano, M.C. Hidalgo, L.A. Rios, J.A. Navío, Appl. Catal. B: Environ. 150–151 (2014) 389.
[19] K.S.W. Sing, D.H. Everett, R.A.W. Haul, L. Moscou, R.A. Pierotti, J. Rouquerol, T. Siemieniewska, Pure Appl. Chem. 57 (1985) 03–619.
[20] B. Ahmmad, K. Kanomata, F. Hirose, Int. J. Chem. Mater. Sci. Eng. 8 (2014) 24.
[21] Z.-M. Dang, L. Wang, L.-P. Zhang, J. Nanomater. 2006 (2006) 1.

[22] C.-Y. Yen, Y.-F. Lin, C.-H. Hung, Y.-H. Tseng, C.-C.M. Ma, M.-C. Chang, H. Shao, Nanotechnology 19 (2008) 045604.
[23] Y. Yu, J.C. Yu, C.-Y. Chan, Y.-K. Che, J.-C. Zhao, L. Ding, W.-K. Ge, P.-K. Wong, Appl. Catal. B: Environ. 61 (2005) 1.
[24] Y. Gao, Y. Masuda, W.-S. Seo, H. Ohta, K. Koumoto, Ceram. Int. 30 (2004) 1365.
[25] V.K.K. Upadhyayula, S. Deng, M.C. Mitchell, G.B. Smith, Sci. Total Environ. 408 (2009) 1.
[26] M. Bonne, S. Pronier, Y. Batonneau, F. Can, X. Courtois, S. Royer, P. Marécot, D. Duprez, J. Mater. Chem. 20 (2010) 9205.
[27] G. Socrates, Infrared and Raman Characteristic Group Frequencies. Tables and Charts, John Wiley & Sons, Ltd., Chichaster, England, 2001.
[28] A. Misra, P.K. Tyagi, P. Rai, D.S. Misra, J. Nanosci. Nanotechnol. 7 (2007) 1820.
[29] M. Scepanovic, M. Grujic-Brojcin, Z.D. Dohcevic-Mitrovic, Z.V. Popovic, Sci. Sinter. 41 (2009) 67.
[30] T. Suzuki, X. Yan, Y. Kitahama, H. Sato, T. Itoh, T. Miura, Y. Ozaki, J. Phys. Chem. C 117 (2013) 1436.
[31] M.S. Dresselhaus, G. Dresselhaus, R. Saito, A. Jorio, Phys. Rep. 409 (2005) 47.
[32] K. Behler, S. Osswald, H. Ye, S. Dimovski, Y. Gogotsi, J. Nanopart. Res. 8 (2006) 615.
[33] G. Jiang, X. Zheng, Y. Wang, T. Li, X. Sun, Powder Technol. 207 (2011) 465.
[34] H. Yu, X. Quan, S. Chen, H. Zhao, Y. Zhang, J. Photochem. Photobiol. Chem. 200 (2008) 301.
[35] Y. Xie, S.H. Heo, S.H. Yoo, G. Ali, S.O. Cho, Nanoscale Res. Lett. 5 (2010) 603.
[36] L.-C. Chen, Y.-C. Ho, W.-S. Guo, C.-M. Huang, T.-C. Pan, Electrochim. Acta 54 (2009) 3884.
[37] Y. Li, X. Li, J. Li, J. Yin, Water Res. 40 (2006) 1119.
[38] T. Jiang, L. Zhang, M. Ji, Q. Wang, Q. Zhao, X. Fu, H. Yin, Particuology 11 (2013) 737.